IEEE Access
Multidisciplinary | Rapid Review | Open Access Journal

Received February 15, 2022, accepted March 7, 2022, date of publication April 5, 2022, date of current version April 13, 2022.

Digital Object Identifier 10.1109/ACCESS.2022.3165121

A Wideband and High-Gain All-Metallic Perpendicular-Corporate-Fed Multi-Layered Parallel-Plate Slot Array Antenna

SHUANG JI, JIRO HIROKAWA, (Fellow, IEEE), AND TAKASHI TOMURA, (Member, IEEE)
Department of Electrical and Electronic Engineering, Tokyo Institute of Technology, Tokyo 152-8552, Japan
Corresponding author: Shuang Ji (ji@antenna.ee.titech.ac.jp)

ABSTRACT An all-metallic multi-layered parallel-plate slot array antenna operated in the 60-GHz band with wide impedance bandwidth and high-gain characteristics is proposed. The 16 × 16-slot antenna is composed of 2 × 2-slot subarrays perpendicularly-fed by a hollow waveguide corporate feeding network. The subarray is partitioned into three functional layers including a bottom one for feeding, a mediate one for radiating and a parasitic one atop for bandwidth enhancement. An undesired resonance of a high-order mode introduced with the parasitic layer is eliminated by loading metal grids between the slotted plates. The contribution of the parasitic layer on bandwidth improvement is verified by a measured 19.2% bandwidth of the antenna with reflection below −10 dB. The removal of the dielectric plate loaded in the conventional double-layered counterpart also contributes to the better performance of the array. The all-metallic feature exempts the design from dielectric loss and beneficial for realizing a higher gain. A high aperture efficiency over 90% is realized over a 19.3% bandwidth and an antenna efficiency over 70% is obtained over a 18.5% bandwidth for the fabricated prototype antennas. The measured realized gain is up to 33.2 dB and the antenna efficiency is 87.2% at 62.0 GHz.

INDEX TERMS Slot array, planar array, parallel-plate waveguide, all-metallic, corporate feed, wideband antenna, high-gain antenna.

I. INTRODUCTION

From millimeter-wave to terahertz band, planar slot waveguide antennas have been one of the most attractive categories due to advantages of high efficiency, compact geometry, easy-to-control aperture distribution and simple installation. They are widely used in applications, such as radars [1], [4], wireless access communication [5], [6], and power transmission systems [7], [8].

In planar arrays, slots are usually etched serially on the walls of hollow rectangular waveguides (HRW), ridged waveguides, post-wall waveguides (PWW, also known as substrate integrated waveguides namely SIW), gap waveguides (GWG), and parallel-plate waveguides (PPW). Proper modes should be excited and fed to slotted parts in these waveguides to finally create a radiation into the free space. Three main schemes to feed are series, corporate, and partially corporate. The series feeds feature shorter path leading to less loss. The corporate feeds feature wide bandwidth at the expense of longer path. Another way to classify the feed topology relies on the positional relationship between the feeding and radiating parts. If both parts are integrated in the same layer, the array is single-layered [9], [12], otherwise multi-layered [13], [14]. The multi-layered ones usually have more compact apertures because the feeding parts are superimposed beneath or over the radiating parts, sharing the same aperture size.

Conventionally, for the multi-layered slot arrays, the perpendicular feed scheme is applied only for propagating energy from the bottom feed waveguide to the upper radiating layer. In the radiating part, the radiation on slot apertures are still excited in serial. Therefore, the array still suffers from long-line effect and limited bandwidth.

In [15], the perpendicular-corporate excitation of multiple radiating elements became feasible. An 8 × 4-way full corporate feed network excites 1 × 2-slot SIW cavities in the

The associate editor coordinating the review of this manuscript and approving it for publication was Davide Ramaccia.

This work is licensed under a Creative Commons Attribution 4.0 License. For more information, see https://creativecommons.org/licenses/by/4.0/

middle layer uniformly, with the two slots exciting a single open-ended cavity in the third layer respectively. However, the array has only 44.4% antenna efficiency at 60 GHz due to high dielectric loss by LTCC technology, despite of a wide 17.1% impedance bandwidth for VSWR < 2.

By HRW, a double-layered array comprising cavity-backed 2×2-slot subarrays perpendicularly-fed by a corporate network was presented in [16]. The four slot elements on the cavity top surface are excited perpendicularly by a shared coupling slot beneath in parallel. The vertical transmission gets more efficient than that in [15] because the middle layer containing power dividers causing extra insertion loss is exempted. The 16×16-slot array shows a measured 12.1% bandwidth for VSWR < 2 and an antenna efficiency high as 83.6% at 61.5 GHz. In [17], the bandwidth was further enhanced to 21.5% by superior design methods.

Thereafter, amounts of slot arrays based on the multi-layered perpendicularly-corporate-fed 2×2-element configuration have been designed by the HRWs [18], [20], PWWs [21], [25], GWGs [26], [30], PPWs [31], [33] or hybrid of them. Except the designs utilizing PPW in the radiating layer, the others all have a cavity section fenced by solid walls, metal posts or pins. And in most cavities, two pairs of inductive stubs formed by solid blocks, posts or pins are embedded to eliminate undesired high-order modes [16], [24],[28]. To obtain a wide impedance bandwidth, various complicated modifications have been made either in the feeds, or radiating elements, or both of them in these designs.

In PWW based designs, [22] and [23] introduce patches as impedance transformers between the feed layer and loaded radiating cavities on the top layer, [25] makes stacked gradually perforated substrates for stepped cavities to better match the impedance with the free space to reduce reflection. Removing a little part of the substrate under slot apertures to tune the Q-value [34] and inserting a via-hole below the slot to introduce one more resonance [35] are also proved to be useful bandwidth enhancing solutions according to researches on single I-shaped narrow slot elements.

In GWG based designs, pins of electromagnetic band gap (EBG) structures constructing the cavity walls [27] are also used to produce tuning effect. Shorter pins between the plates yielding capacitance can contribute to significant bandwidth enhancement both in power dividing junctions [28] and cavity subarrays [29]. For ridge GWG feeds, more complex ridge terminals engender better matching effect as well [26], [27],[29], [30].

For designs utilizing the PPW in the feed part, in [31], although four blocks were used in the radiating cavities to improve bandwidth and polarization discrimination of the subarrays, the realized bandwidth for VSWR < 2 of the complete array was only about 6% because the subarrays were fed serially by the plane waves in the folded PPW network. For designs utilizing the PPW in the radiating parts, the cavity walls are exempted and no vertical structures exist between the parallel plates. To enhance the bandwidth, loading parasitic slotted plates was presented as a solution. However, despite of superimposed third, or fourth slotted plates added over the basic double-layered PTFE-loaded arrays, the bandwidth enhancement in [32] and [33] was moderate. Furthermore, owing to air slits between stacked copper and PTFE plates in assembly, the equivalent relative permittivity of the parallel-plate region deviated, the measured bandwidth and efficiency degraded a lot from the simulated ones.

In this manuscript, based on the perpendicularly-corporate-fed 2×2-element configuration, an all-metallic triple-layered 16×16-slot array composed of PPW-based radiating part and HRW-based feeding part is proposed. In the corporate feed circuit made mainly from cascading HRW power dividers, the transitional structure bridging the dividers and the feed port is modified into a stepped type, to realize a wider bandwidth of the feed part. In the radiating part, no dielectric substrate is loaded, different from the conventional designs in [32] and [33]. With a simpler triple-layered all-metallic geometry, the proposed subarray realizes a wider impedance bandwidth and higher efficiency, indicating a new feasible solution different from the conventional designs. Namely, the PPW based subarrays without an integrated substrate can achieve a comparable or even better performance compared to conventional substrate-loaded designs. The removal of the substrate will not only ease the antenna from significant deterioration of performance due to assembly error occurred in [32] and [33], but also facilitate this type of antenna to work in temperature-sensitive environment where no substrate is preferred. Ultimately, the proposed array antenna combines advantages of wide impedance bandwidth, high-gain, high-efficiency, and simple geometry in a balanced way, verified by measured results.

II. CONFIGURATION OF ANTENNA

The geometry of the all-metallic triple-layered parallel-plate 16×16-slot array antenna is illustrated in Fig. 1. The copper plates are categorized into three layers numbered as #1-#3 from the bottom up. A 64-way corporate feed circuit composed of 6-level cascading T-junction equal power dividers is designed in Layer #1 by laminated diffusion-bonded plates, with one feed aperture for WR-15 waveguide at the back and uniform 8×8 coupling slot apertures atop. Above these are separate plates that are stacked together and fastened by screws at corners. An air layer braced by a frame and a plate with uniformly arrayed 16×16 radiating slots constitute Layer #2. The remains belong to the parasitic layer #3. In the air region between the radiating slot plate and the similar parasitic slotted plate, there is an intermediate grid layer comprising evenly-spaced thin strips distributed in parallel, with equal vertical distance from the both plates. The wave propagates perpendicularly across the layers and form a boresight radiation.

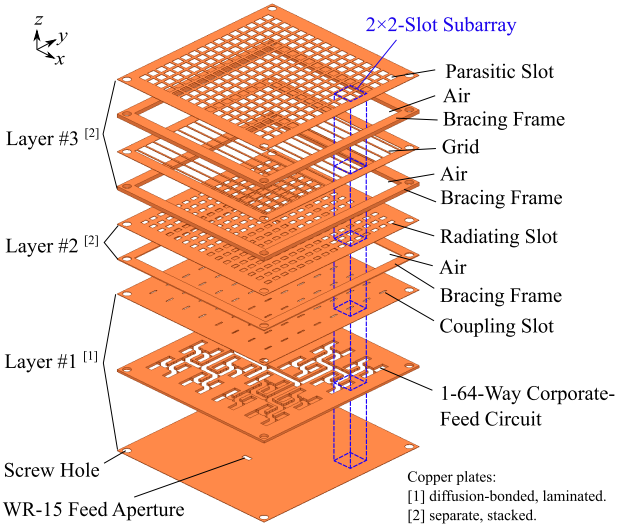

FIGURE 1. Exploded view of the 16 × 16-slot array antenna.

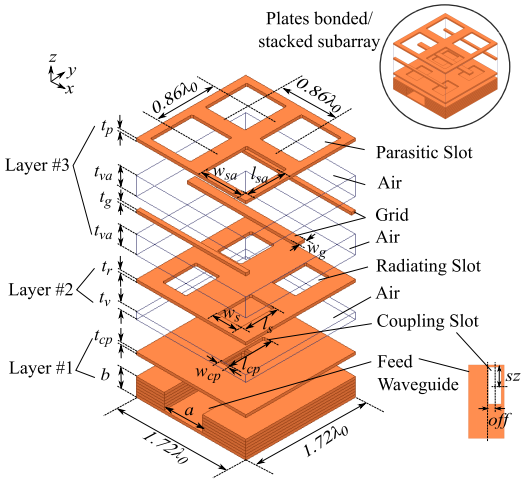

FIGURE 2. Exploded view of the 2 × 2-slot subarray.

III. DESIGNS OF SUBARRAY AND FEED NETWORK

A. WIDEBAND AND HIGH-GAIN TRIPLE-LAYERED PARALLEL-PLATE 2×2-SLOT SUBARRAY

As shown in Fig. 2, a single square 2 × 2-slot subarray (size: $1.72\lambda_0 \times 1.72\lambda_0$, where λ_0 is the free space wavelength at the design frequency of 61.5 GHz) extracted from the periodic array includes all three layers. In Layer #1, a straight short-ended rectangular waveguide is modeled, as a simplified alternative of the practical last-level half T-junction of the feed circuit. A rectangular coupling slot is set on the top widewall with an offset from the waveguide symmetrical plane. In Layer #2, there are 2 × 2 rectangular slots of the same dimensions allocated uniformly on the top plate. The Layer #3 has an analogous composition as the Layer #2, except that there is a grid located at the central height of the parallel-plate region. With a spacing of half periodicity of the subarrays, thin strips parallel to polarization direction are arranged evenly along the cross-polarized direction.

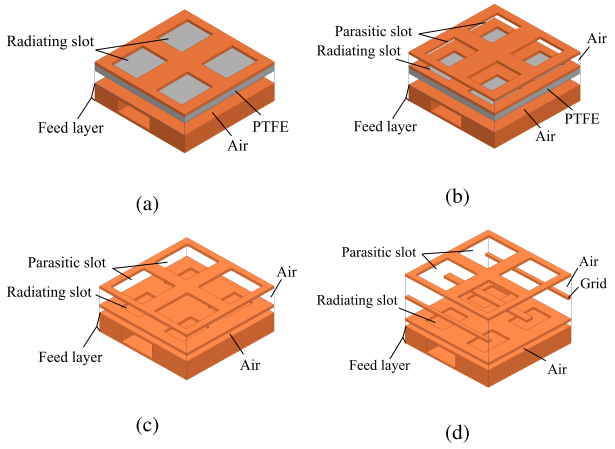

FIGURE 3. Parallel-plate subarrays, (a) double-layered with substrate [36], (b) triple-layered with substrate [37], (c) triple-layered all-metallic, (d) triple-layered all-metallic with grid (the proposed).

The proposed subarray went through several innovations mainly in the radiating part as illustrated in Fig. 3, from a conventional double-layered design with a dielectric substrate (PTFE, $\varepsilon_r = 2.17$, thickness = 0.254 mm) to the present triple-layered all-metallic one [36], [37]. Firstly, [36] analyzed the double-layered PTFE-loaded model shown in Fig. 3 by a computational method. The optimum dimensions realizing an impedance bandwidth of 13.2% for VSWR < 1.5 were obtained by running a genetic algorithm based on the analysis. To further enhance the bandwidth, a third parasitic slotted plate was set on the top of the basic double-layered model with an air layer beneath, forming the third layer, as shown in Fig. 3b. It was optimized by the same methods and shows an optimum bandwidth of 16.0% [37].

1) ADDITION OF THE PARASITIC THIRD LAYER

The influence of loading a parasitic plate atop is illustrated firstly in this manuscript by the eigenmode analysis on models in Fig. 3(a) and Fig. 3(b). The optimum parameters of the double-layered and triple-layered subarrays with substrate loaded are listed in TABLE 1. Since both subarrays are geometrically symmetric, we can extract a quarter part of the radiating part respectively, namely one slot element, and apply proper boundary conditions, as shown in Fig. 4, to compare the eigemodes generated. For the coupling slot, perfect electrical conductor (PEC) boundary is set on the symmetrical plane perpendicular to the slot transverse direction, and perfect magnetic conductor (PMC) boundary is set on the symmetrical plane perpendicular to the longitudinal direction. In the radiating part, two pairs of periodic boundary condition (PBC) boundaries are applied on the peripheries, and perfect matching layer (PML) boundary is set atop with a distance of λ_0 from the top slot aperture.

The electrical field distribution on the parasitic and coupling slot apertures of two effective modes in the triple-layered model are plotted in Fig. 5, with corresponding

TABLE 1. Parameters of the substrate-loaded double-layered and triple-layered subarrays (Unit: mm).

Component	Layer #1						Layer #2		
Parameter	a	b	off	sz	w_{cp}	l_{cp}	t_v	w_r	l_r
2-layered	2.95	1.00	0.55	1.64	1.06	2.93	0.51	2.74	2.93
3-layered	2.95	1.00	0.49	1.58	0.88	2.85	0.55	2.61	2.58
Component	Layer #3			Plate thickness					
Parameter	t_{va}	w_{sa}	l_{sa}	t_{cp}	t_r	t_p			
3-layered	1.10	2.65	2.82	0.20					

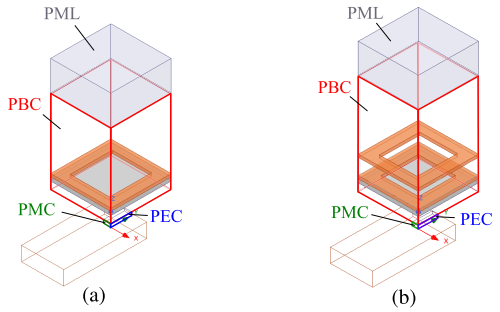

FIGURE 4. Quarters of subarrays in eigenmode anlysis.(a) double-layered with substrate, (b) triple-layered with substrate.

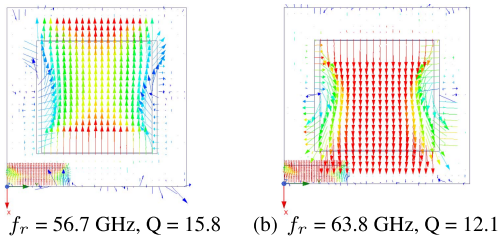

FIGURE 5. Electrical field distributions of two eigenmodes on the coupling and parasitic slot apertures in the conventional substrate-loaded triple-layered subarray, (a) first mode, (b) second mode.

low Q-values (quality factors) and resonant frequencies in the band from 54 GHz to 68 GHz. The influence of the third layer on the bandwidth is shown by comparing the frequency characteristics of reflection of the double-layered and triple-layered subarrays in Fig. 6. The star marks denote the allocations of the resonant eigenmodes contributing to radiation in respective model. The triple-layered model has one more mode resonating in high frequency band at 63.8 GHz. Its first mode also resonates at lower frequency point than that of the double-layered model, thus expanding the frequency span where the VSWR of the subarray is less than 1.5. It is verified that the introduction of the third layer facilitates a wider impedance bandwidth. Gain of the triple-layered subarray also sees an increase from that of the double-layered one, especially around the two eigenmode resonant frequency points, as displayed in Fig. 7.

It is proved that loading a parasitic plate works for enhancement of bandwidth but the effect is still modest. Instead of adding more layers as in [32] and [33], this manuscript presents a different proposal removing the substrates between the plates. The following work shows that the dielectric

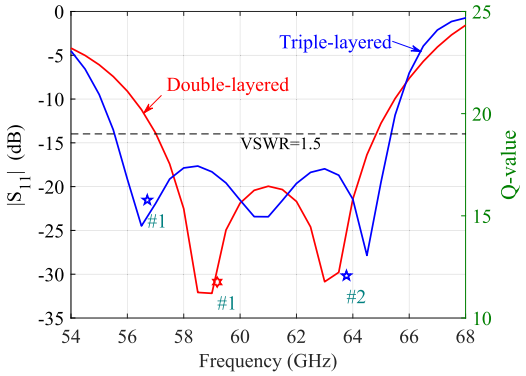

FIGURE 6. Frequency characteristics of reflection and key eigenmodes of conventional substrate-loaded double-layered and triple-layered parallel-plate 2 × 2-slot subarrays.

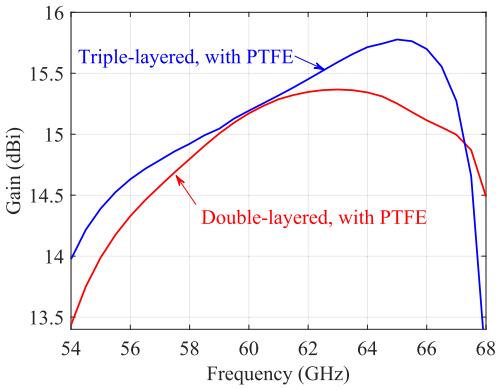

FIGURE 7. Gain of conventional double-layered and triple-layered parallel-plate 2 × 2-slot subarrays (with substrate).

substrate is not necessary between the plates for such a parallel-plate design. Furthermore, along with the removal of the substrate beneath the radiating slots, reduced dielectric loss will lead to higher radiation efficiency. The triple-layered all-metallic model shown in Fig. 3(c) was firstly analyzed and optimized based on the same computational methods utilized in [37]. However, occurrence of undesired high-order modes in the parasitic third layer for the all-metallic designs is inevitable. Since there are no stubs or pins between plates depressing high-order modes as the other cavity-backed designs, to address this problem, the grid-loaded model shown in Fig. 3(d) is proposed. The mechanism and effect of loading the grid between the plates are clarified as follows.

2) REMOVAL OF SUBSTRATE IN THE SECOND LAYER AND INTRODUCTION OF GRID IN THE THIRD LAYER

Eigenmode analysis was conducted on the all-metallic triple-layered subarray in Fig. 3(c) and two eigenmodes were discovered. The first mode resonates at 57.5 GHz with a Q-value of 14.9, and the second resonates at 64.9 GHz with a Q-value of 12.0. Both resonances shifted to higher frequency points compared to those of model in Fig. 3(b). As a result, the reflection level still stays low and the gain remains high up to 67 GHz, as shown in Fig. 8.

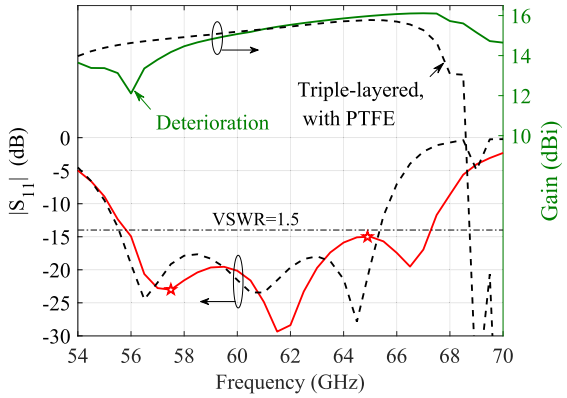

FIGURE 8. Gain and reflection of triple-layered all-metallic parallel-plate 2 × 2-slot subarray.

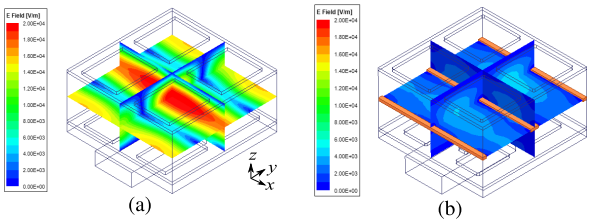

FIGURE 9. Electrical field distributions on the symmetrical planes of the air region in the third layer at 56.5 GHz. (a) All-metallic triple-layered subarray without grid, (b) all-metallic triple-layered subarray with grid (proposed).

However, it can be observed that at about 56.0 GHz, deterioration of the gain occurs. It results from an intensive resonance of a high-order mode in the air region of the Layer #3. The electrical field distributions on the symmetrical planes of the region at 56.5 GHz are displayed in Fig. 9. In Fig. 9(a), the field intensity is strong at the positions where three thin grid strips are inserted as shown in Fig. 3(d). Most energy is stored in the region and unable to be radiated. Thus, by loading the grid into the subarray, the boundary condition forces the tangential components of electrical fields on the metal conductors to be zero so that the intensive electrical fields along the strips are eliminated and the mode is removed, as illustrated in Fig. 9(b). As the fields at this frequency point in the proposed model gets weaker, the power flows mainly upward to the free space, and finally the realized gain is possible to restore to a normal level denoted by the red curve in Fig. 10.

The parameters in the proposed all-metallic grid-loaded parallel-plate slot subarray are tabulated in TABLE 2. Its frequency characteristics of gain and reflection are shown by red curves in Fig. 10, with comparison to the other two conventional triple-layered designs depicted in Fig. 3(b) and Fig. 3(c). The subarray has reflection below −14 dB (VSWR < 1.5) from 56.0 GHz to 67.5 GHz, realizing an impedance bandwidth of 18.6%, not only much enhanced from the 7.7% of the triple-layered parallel-plate designs in [31], but also improved from the 13.1% (57.0 GHz to

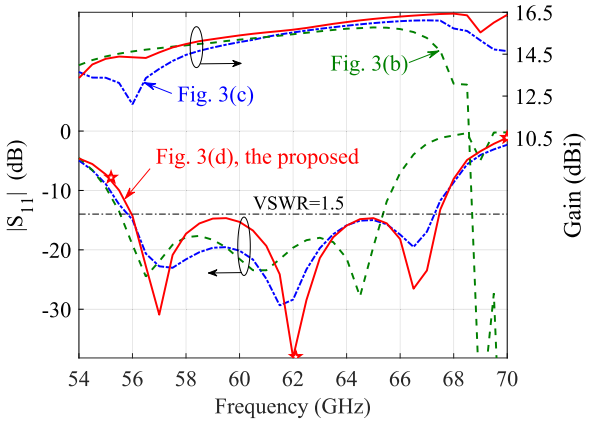

FIGURE 10. Gain and reflection of the proposed all-metallic grid-loaded triple-layered parallel-plate 2 × 2-slot subarray.

TABLE 2. Parameters in the proposed all-metallic grid-loaded parallel-Plate slot subarray (Unit: mm).

Component	Layer #1						Layer #2		
Parameter	a	b	off	sz	w_{cp}	l_{cp}	t_v	w_r	l_r
Proposed	2.95	1.20	0.59	1.86	0.64	3.36	0.50	1.83	2.60
Component	Layer #3				Plate thickness				
Parameter	t_{va}	w_{sa}	l_{sa}	w_g	t_{cp}	t_r	t_g	t_p	
Proposed	1.90	3.08	3.21	0.60	0.20				

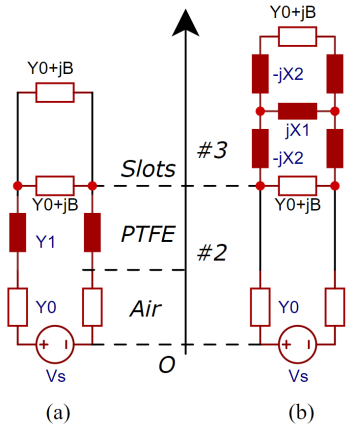

FIGURE 11. Transverse equivalent networks for radiating parts comprised of Layer #2 and Layer #3 of the triple-layered (a) conventional substrate-loaded subarray, and (b) proposed all-metallic grid-loaded subarray.

65.0 GHz) in [36] and 16.0% (55.5 GHz to 65.1 GHz) in [37] realized by the authors. Moreover, the high-gain band is also extended especially at the high frequency end.

The design of the all-metallic subarray in Fig. 3(c) was realized by the same methods introduced in [36]. The proposed grid-loaded subarray in this manuscript shown in Fig. 3(d) is designed by the ANSYS HFSS simulations.

3) PHYSICAL INTERPRETATION BY EQUIVALENT NETWORKS

The parallel-plate 2 × 2-slot subarrays in Fig. 3 can be regarded as uniform planar leaky-wave antennas featuring

a broadside radiation [38]. The slotted plates in the radiating parts can be modeled as a partially reflecting surface and represented by a shunt susceptance denoted as jB [39]. Transverse equivalent networks for radiating parts comprised of Layer #2 and Layer #3 of the triple-layered conventional substrate-loaded subarray shown in Fig. 3(b) and the proposed all-metallic grid-loaded subarray shown in Fig. 3(d) are modeled in Fig. 11.

The radiating parts are excited by the electrical fields or equivalent magnetic currents on the coupling slot. This source is modeled as a voltage source V_s. Y_0 and Y_1 are the admittances in the air and dielectric regions, respectively. With the removal of the dielectric substrate, Y_1 $(= G_1 + jB_1)$ disappears. The introduction of the grids replenishes the effects of this change and makes the impedance matched again. Because the strips of the grids are parallel to the polarization direction, they are inductive and can be represented by a reactance jX_1. Take the thickness of these strips into account, capacitive $-jX_2$ are cascaded into the circuit [40]. There is a minus in this item, so it can be equivalent to a capacitive susceptance jB_2. Their series connection with the remained network makes compensation for the eliminated imaginary component jB_1. The shunt connection of them and jX_1 with the remained network compensates for the eliminated real component G_1.

B. CORPORATE-FEED NETWORK

Besides the wideband subarrays, the feed network should also be wideband for good performance of the full array. For the 64-way corporate feed circuit, reflection performance of the cascading power dividers and the transitional E-bend section should both be optimized to guarantee a low level at least within the impedance bandwidth of the subarrays.

The description of the junction power dividers can be found in [16] and [38]. An 18.1% fractional bandwidth (55.7 GHz to 66.8 GHz) with reflection below −25 dB is realized here for the last level H-junction divider (composed of two back-to-back T-junctions).

As to the E-bend transition, the proposed structure of the E-bend connecting to the first level T-junction is shown in Fig. 12, together with a conventional one. In the conventional design, a short-end waveguide branch with wider broad wall is set above the WR-15 aperture, playing the role of matching impedance between the feed port and the branch of next power divider. At the discontinuous joints of the branches, pairs of inductive windows or irises and inductive walls are set up to yield reactant tuning effects. Wide bandwidth can be achieved by introducing more branches with gradually sized wide walls. In the proposed design, instead of multiple cascading branches of staged wide wall sizes in the H-plane, several steps are utilized directly connecting the WR-15 aperture and the trunk of the first T-junction, to match the impedance. Three steps are designed here. More steps will lead to more fabrication cost. The height of the steps should be multiple of plates thickness from the beginning of design for sake of fabrication. The parameters of the proposed

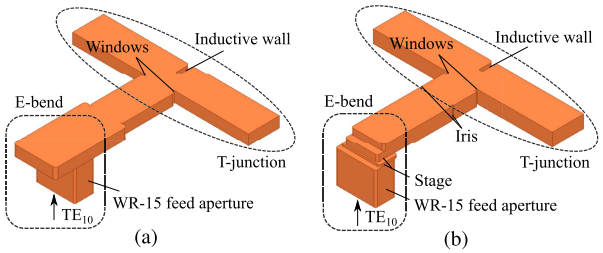

FIGURE 12. E-bend with the first T-junction divider. (a) conventional [35]. (b) proposed.

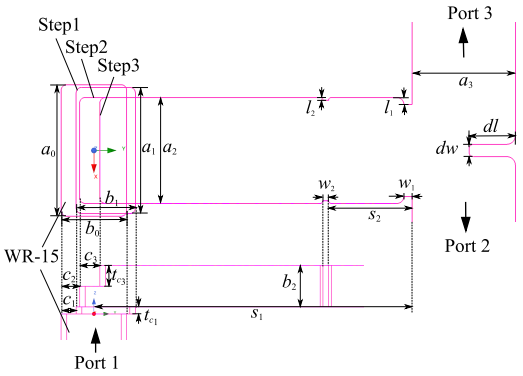

FIGURE 13. Parameters of the proposed E-bend with the first level T-junction power divider (top and section views): $a_0 = 3.76$, $a_1 = 3.72$, $a_2 = 3.01$, $a_3 = 2.96$, $b_0 = 1.88$, $b_1 = 1.91$, $b_2 = 1.20$, $c_1 = 0.34$, $c_2 = 0.55$, $c_3 = 0.56$, $s_1 = 9.13$, $s_2 = 2.72$, $t_{c1} = 0.20$, $t_{c3} = 0.60$, $dw = 0.35$, $dl = 1.33$, $w_1 = 0.24$, $l_1 = 0.19$, $w_2 = 0.15$, $l_2 = 0.08$, unit: mm.

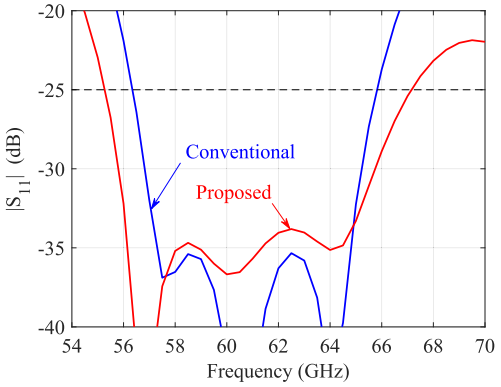

FIGURE 14. Comparison of performance between the conventional and proposed E-bend transitional structures connecting to a T-junction divider.

model are shown in Fig. 13. The frequency characteristics of the two types of E-bends connected to a T-junction are shown in Fig. 14. The impedance bandwidth with reflection less than −25 dB is improved from the conventional 15.5% (56.3 GHz to 65.8 GHz) to 19.4% (55.3 GHz to 67.1 GHz), larger than the bandwidth of the aforementioned subarray or H-junction.

The reflection performance the feed part including the transitional structure is shown in Fig. 15. A bandwidth of 17.5% with level below −25 dB is obtained from 55.8 GHz to 66.5 GHz, owing to the low reflection of each component.

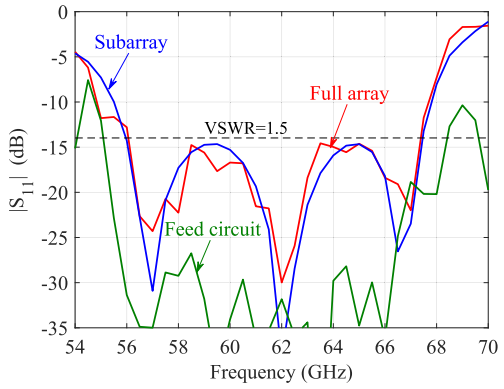

FIGURE 15. Simulated frequency characteristics of reflection of the proposed full structure all-metallic parallel-plate 16 × 16-slot array.

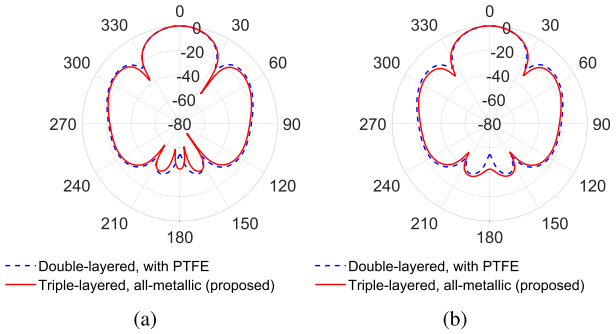

FIGURE 16. Simulated radiation patterns in the (a) E-planes and (b) H-planes of conventional double-layered substrate-loaded and proposed triple-layered all-metallic grid-loaded 2 × 2-slot subarrays at 61.5 GHz.

C. SIMULATED RESULTS OF ARRAY ANTENNA

With arrayed subarrays along both axes of an orthogonal coordinate system to form a 16 × 16-slot scheme, fed by the 64-way corporate network, excited via a standard WR-15 waveguide aperture, the full antenna shows simulated reflection performance plotted in Fig. 15. An 18.2% bandwidth for VSWR < 1.5 from 56.1 GHz to 67.3 GHz is acquired. And according to the comparison between the feed and the subarray, the bandwidth of the array antenna is consistent with and mainly restricted by that of the subarray. In the simulation, the metal plates are assumed as copper (the conductivity: 5.8×10^7 S/m), and all slots are chamfered in consideration of fabrication.

Figure 16 displays comparison of simulated radiation patterns between the conventional double-layered substrate-loaded and the proposed triple-layered all-metallic grid-loaded 2 × 2-slot subarrays at 61.5 GHz. Figure 17 displays those of corresponding 16 × 16-slot arrays. Because the subarrays are deployed in the same uniform distribution pattern with the same periodicity, the array factors are the same. The radiation pattern of the array is the product of the array factor and subarray radiation pattern. In Fig. 16, main lobes of subarrays are almost similar in both planes, except the depth of first nulls and angular positions have a little difference. The first nulls of the proposed subarray locates at $\theta = \pm 35°$, so the proposed array realizes nulls at these positions, exempted from the high grating levels observed in the conventional design.

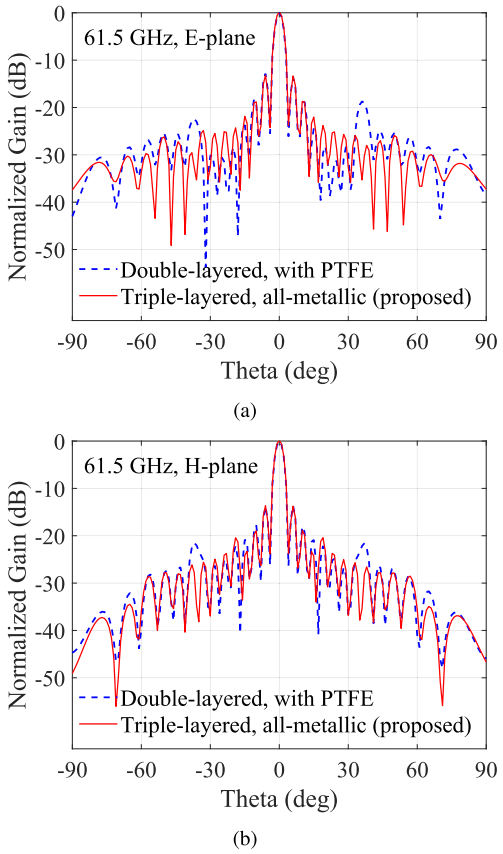

FIGURE 17. Simulated radiation patterns in the (a) E-planes and (b) H-planes of conventional double-layered substrate-loaded and proposed triple-layered all-metallic grid-loaded 16 × 16-slot arrays at 61.5 GHz.

IV. FABRICATION AND MEASURED RESULTS

A. FABRICATION

Two same array antennas are fabricated numerated as Ant. 1 and Ant. 2. The components and assembled array antenna are shown in Fig. 18. At fringes of the array, margins of around one wavelength (4.0 mm-wide in the *xoz*-plane and 4.8 mm-wide in the *yoz*-plane) are set for convenience of assembly. At the four corners of all plates, screws holes are preset. Plates of Layer #2 and Layer #3 are tightly stacked and connected to Layer #1 by screws. Diffusion bonding technology is utilized for the fabrication of Layer #1, providing a foundation of reliable performance of the hollow waveguide feed network [41]. The copper plates used have thickness of 0.2 or 0.3 mm. The thickness of each component and plate allocation are written in corresponding brackets in Fig. 18. For those sections where only air exists, copper margin frames furnish bracing. In the *yoz*-plane, the dimension of the air section will be prolonged for around $1/4\lambda_0$ (1.3 mm) to maintain a proper boundary condition for subarrays at the verge. Base on previous experience, over-etching error of

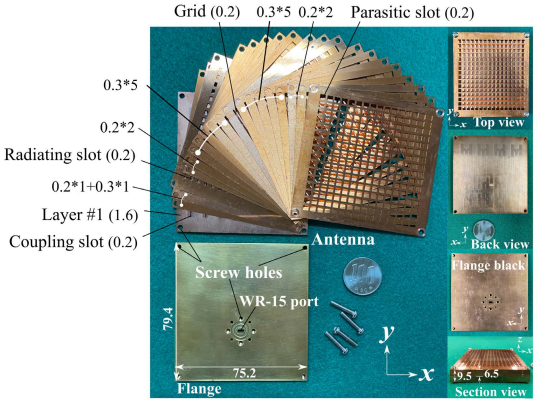

FIGURE 18. Fabricated array antenna with flange (Unit: mm).

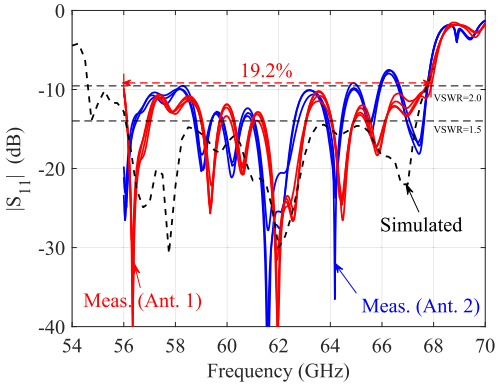

FIGURE 19. Measured frequency characteristics of reflection of full structure all-metallic grid-loaded parallel-plate 16 × 16-slot arrays.

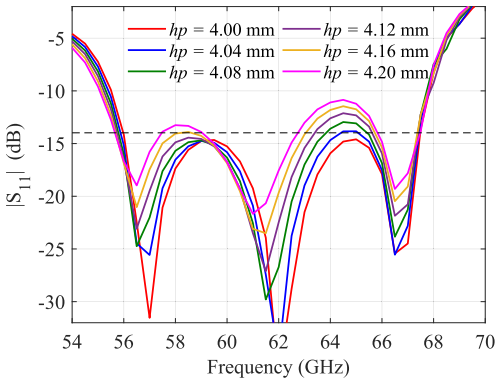

FIGURE 20. Influence of error in air thickness (*hp*) in Layer #3 on the reflection characteristic of the subarray.

0.02 mm is assumed for all slots in wet-etching process and it is compensated in advance.

B. MEASURED RESULTS

1) REFLECTION

The measured frequency characteristics of reflection of both antennas are plotted in Fig. 19, in comparison with the simulated result. The curves start from 56.0 GHz due to the limitation of the available band of the vector analyzer.

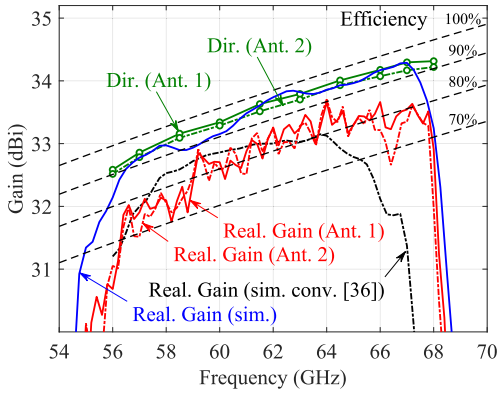

FIGURE 21. Measured directivity and realized gain of full structure all-metallic gird-loaded parallel-plate 16 × 16-slot arrays.

The measured reflection coefficients in dB of both antennas degrade from the simulated a little, but still in general agreement with it on positions of peaks and nulls. A measured impedance bandwidth up to 19.2% for VSWR < 2.0 is realized from 56.0 GHz to 67.9 GHz. It is almost of the same range as the simulated bandwidth for VSWR < 1.5.

It can be observed that significant deviation in refection levels mainly locates at points around 58.0 GHz and 67.0 GHz, where two resonances of the subarray exist and relatively high reflections occur in the feed circuit (in Fig. 15). Therefore, the error could either come from the subarrays or the feed part. To figure it out, parametric analysis is conducted on the radiating part firstly. It turns out that there is high possibility that the error in height of the air region in Layer #3 led to this deterioration. As shown in Fig. 20, as the thickness *hp* of air ($hp = 2t_{va} + t_g$) increases, the reflection level of the subarray will get higher in the band, especially around 58.0 GHz and 64.5 GHz. Besides this, two nulls in reflection levels around 57.0 GHz and 62.0 GHz are observed to shift a little to the lower frequencies. Identical phenomenon can be seen from the results of the measure arrays. This error may come from the deformation of the plates (especially the one atop with parasitic slots) because they are attached by only four screws at the array corners. If the screws are fastened too tight, factual height of the air region may get larger than the designed value. Adding more screws at the margins will assure better flatness and reduce this error. Secondly, according to the performance of feed part shown in Fig. 15, if the reflection levels at 58.0 GHz and 67.0 GHz are further depressed in case of any error introduced by fabrication, the reflection performance of the arrays displayed in Fig. 19 will get improved and more closed to the simulated one as well.

2) DIRECTIVITY, GAIN AND EFFICIENCY

The measured directivity and realized gain of antennas are plotted in Fig. 21 with efficiency. The simulated realized gain of the proposed array shows significant gain enhancement in comparison to the conventional double-layered substrate-loaded array. It is resulted from the widened bandwidth and

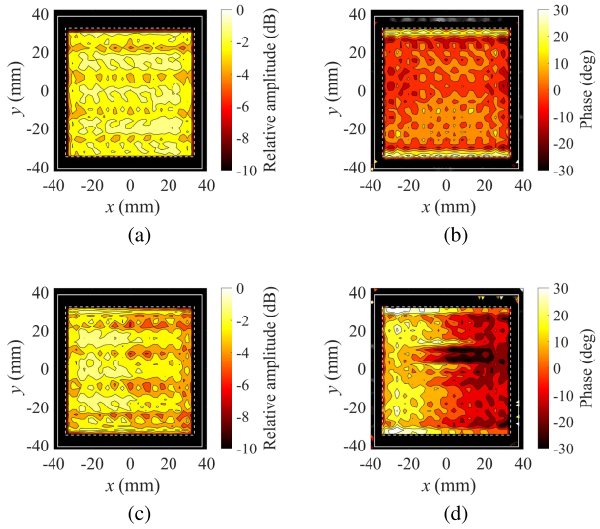

FIGURE 22. Relative electrical field distribution on the antenna apertures at 61.5 GHz, of Ant. 1 (a) amplitude, (b) phase, Ant. 2 (c) amplitude, (d) phase.

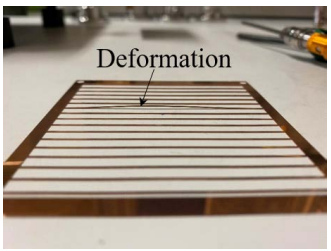

FIGURE 23. Deformation of a strip in the grid of Ant. 2.

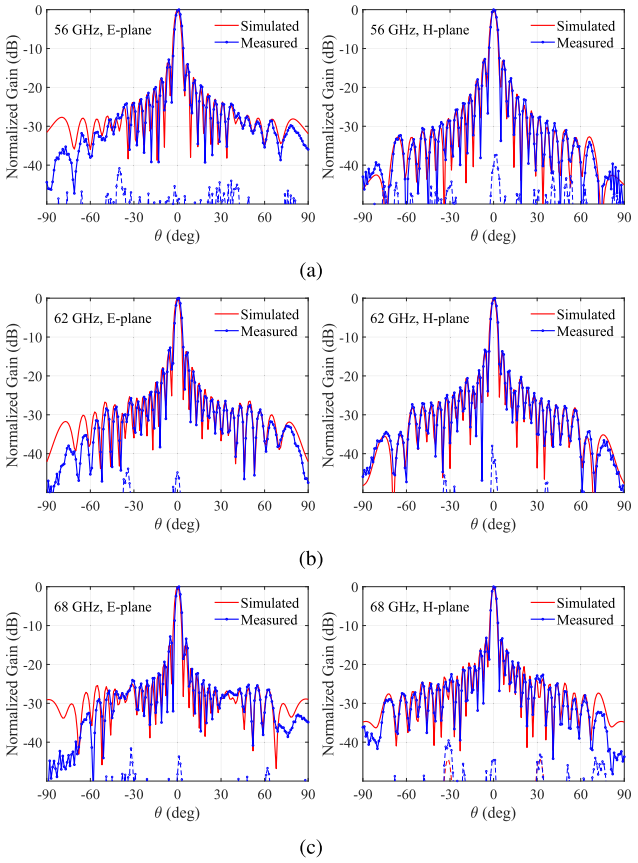

FIGURE 24. Measured and simulated radiation patterns in the E-plane and H-plane of Ant. 1 at (a) 56.0 GHz, (b) 62.0 GHz, and (c) 68.0 GHz.

reduced dielectric loss of the proposed subarray. The measured directivity keeps high in the whole band, indicating a high aperture efficiency over 90%. The measured realized gain (conductor and mismatch loss included) is about 0.5 dB less than the simulated in average, which is acceptable. Larger deviation from 57.0 GHz to 59.0 GHz corresponds to the aforementioned deterioration in reflection among this frequency range. The antenna has antenna efficiency above 70% almost in the whole impedance bandwidth. At the centered 62.0 GHz (f_c), the realized gain of the array is 33.2 dB and antenna efficiency is 87.2%.

3) NEAR-FIELD DISTRIBUTION

The relative amplitudes of electrical fields distributed over the antenna apertures at the designed frequency 61.5 GHz are illustrated in Fig. 22. The fields are generally uniform among the periodic subarray apertures both in amplitude and phase. There is some variation in phase at the fringes in the *yoz* plane (H-plane) due to the difference of boundary conditions from the assumed periodic boundaries of a single subarray, as the array is finite. For Ant. 2, a deformation of one strip in the grid plate took place accidentally as shown in Fig. 23, accounting for the degradation of uniformity of the field distribution.

4) RADIATION PATTERNS

The measured radiation patterns of the fabricated antennas in E-plane (*xoz*-plane), H-plane (*yoz*-plane) are given in Fig. 24 and Fig. 25 at 56.0 GHz, 62.0 GHz, and 68.0 GHz. Good agreement is achieved in both planes between the measured and simulated results. The measured cross polarization levels also stay at low levels below −40 dB, as shown by the dashed curves. The agreement between simulated results and symmetry of patterns got a little worse for Ant. 2 than Ant. 1 because of the aforementioned deformation of one strip. The field radiation pattern of Ant. 1 at the 45°-plane at 62.0 GHz is shown in Fig. 26. The difference between the simulated and the measured sidelobe levels around $\theta = 55°$ may come from a slight plane misalignment of several degrees in the measurement.

C. DISCUSSION

The measured results verified the wideband, high-gain, and high-efficiency features of the proposed all-metallic parallel-plate 16×16-slot array antenna. A comparison conducted between the several conventional planar slotted arrays working in the V- and E-band based on similar perpendicularly-corporate-fed 2×2-element configurations are listed in TABLE 3. Compared with varies conventional

TABLE 3. Comparison of planar slotted array antennas with perpendicularly-fed 2 × 2-element subarrays designed in V- or E-band.

Ref.	Subarray Geometry	Waveguides	Antenna Size ($\times\lambda_0$)	Elements	Freq. (GHz)	BW	Gain$_{f_c}$ (dBi)	Efficiency$_{f_c}$
[16]	X-shaped cavity	HRW	15.4×15.6×0.6	16×16	58– 65.5	12.1%	33.5	83.6%
[17]	X-shaped cavity	HRW	15.4×15.6×0.7	16×16	54.7– 67.8	21.5%	32.6	76.5%
[19]	X-shaped cavity	HRW	26.8×26.8	32×32	71.0– 86.5	19.7%	38.1	72.0%
[22]	cavity-patch-cavity	SIW	12.2×13.6×0.8	16×16	57.5– 67.0	15.3%	28.9	37.4%
[23]	cavity-patch-cavity	SIW	12.7×17.9×0.78	16×16	71.0– 88.5	22.0%	30.1	36.0%
[27]	X-shaped cavity	GWG	16.4×16.4×2.5	16×16	56.0– 65.7	15.9%	32.6	78.0%
[28]	X-shaped cavity	GWG	16.4×16.4×2.5	16×16	55.5– 67.0	18.8%	32.9	82.0%
[29]	X-shaped cavity	GWG	9.2×9.2×2.8	8×8	50.0– 67.8	30.0%	27.2	82.5%
[32]	Parallel-plate, substrate-loaded	PPW	16.6×16.2×0.7	16×16	NA	NA	31.7	61.0%
[33]	Parallel-plate, substrate-loaded	PPW	16.8×16.3×1.1	16×16	60.8- 66.0	8.2%	32.7	75.5%
[36]	Parallel-plate, substrate-loaded	PPW	16.3×15.4×0.5	16×16	58.7- 67.0	13.2%	32.9	81.8%
Proposed	Parallel-plate, all-metallic	PPW	16.3×15.4×1.3	16×16	56.0- 67.9	19.2%	33.2	87.2%

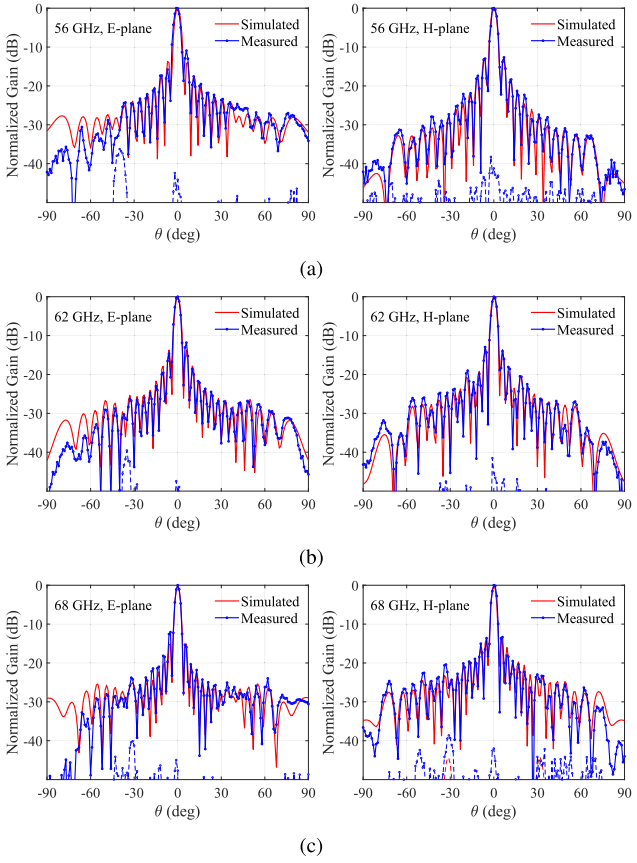

FIGURE 25. Measured and simulated radiation patterns in the E-plane and H-plane of Ant. 2 at (a) 56.0 GHz, (b) 62.0 GHz, and (c) 68.0 GHz.

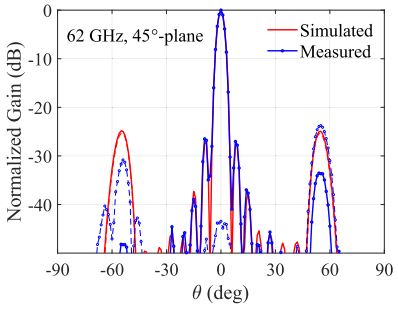

FIGURE 26. Radiation pattern of Ant. 1 at the 45°-plane at 62.0 GHz.

complicated cavity-backed designs and parallel-plate designs with dielectric substrate loaded, the proposed all-metallic design still stands out by its simple geometry and good electrical performance.

V. CONCLUSION

Based on the 2 × 2-slot multi-layered parallel-plate subarray perpendicularly-fed by waveguide corporate feeding network, a 16 × 16-slot all-metallic array antenna is designed, fabricated and measured. Wide impedance bandwidth up to 18.6% for VSWR < 1.5 and high-gain characteristics are obtained by applying a parasitic layer on the top and removing a substrate between plates in the subarray. A grid layer constituted of thin strips is loaded between the plates to remove undesired high-order mode resonance which imposes negative influence on radiation. The feed circuit especially the E-bend transitional part is modified from conventional designs into a stepped type for wider impedance bandwidth as well. The measured antennas prove a 19.2% bandwidth for VSWR < 2.0 and high antenna efficiency over 70% in the band from 56.0 GHz to 67.9 GHz. The difference between the measured and the simulated reflection levels mainly results from deformation of the thin top plate after assembly. Setting more screws at the margins will reduce the error. For one fabricated prototype, the measured realized gain is 33.2 dB and antenna efficiency is 87.2% at 62.0 GHz. The all-metallic parallel-plate radiating parts are easy to fabricate and convenient to be slot-coupled by other types of transmission lines besides the hollow waveguides used in this design. It is the first realization of such a parallel-plate all-metallic slot array antenna, of which geometric simplicity, wideband and high efficiency characteristics are demonstrated simultaneously.

REFERENCES

[1] W. Menzel and A. Moebius, "Antenna concepts for millimeter-wave automotive radar sensors," *Proc. IEEE*, vol. 100, no. 7, pp. 2372–2379, Jul. 2012.

[2] H. Kirino and K. Ogawa, "A 76 GHz multi-layered phased array antenna using a non-metal contact metamaterial waveguide," *IEEE Trans. Antennas Propag.*, vol. 60, no. 2, pp. 840–853, Feb. 2012.

[3] L. Qin, Y. Lu, Q. You, Y. Wang, J. Huang, and P. Gardner, "Millimeter-wave slotted waveguide array with unequal beamwidths and low sidelobe levels for vehicle radars and communications," *IEEE Trans. Veh. Technol.*, vol. 67, no. 11, pp. 10574–10582, Nov. 2018.

[4] Y. Yu, W. Hong, H. Zhang, J. Xu, and Z. H. Jiang, "Optimization and implementation of SIW slot array for both medium and long-range 77 GHz automotive radar application," *IEEE Trans. Antennas Propag.*, vol. 66, no. 7, pp. 3769–3774, Jul. 2018.

[5] F. Manzillo, M. Ettorre, and M. Lahti, "A multilayer LTCC solution for integrating 5G access point antenna modules," *IEEE Trans. Microw. Theory Techn.*, vol. 64, no. 7, pp. 2272–2283, Jul. 2016.
[6] Z.-C. Hao, H.-H. Wang, and W. Hong, "A novel planar reconfigurable monopulse antenna for indoor smart wireless access points' application," *IEEE Trans. Antennas Propag.*, vol. 64, no. 4, pp. 1250–1261, Apr. 2016.
[7] B. Yang, X. Chen, J. Chu, T. Mitani, and N. Shinohara, "A 5.8-GHz phased array system using power-variable phase-controlled magnetrons for wireless power transfer," *IEEE Trans. Microw. Theory Techn.*, vol. 68, no. 11, pp. 4951–4959, Nov. 2020.
[8] W. Lin and R. W. Ziolkowski, "High directivity, omnidirectional horizontally polarized antenna array for wireless power transfer in Internet-of-Things applications," in *Proc. Eur. Conf. Antennas Propag.*, Mar. 2020, pp. 11–14, Mar. 2020.
[9] K. Hashimoto and M. Higaki, "Practical design of radiating part of post-wall waveguide-fed parallel plate slot array antenna by method of moments," in *Proc. 14th Eur. Conf. Antennas Propag. (EuCAP)*, Mar. 2020, pp. 1–5.
[10] K. Gong, Z. N. Chen, X. Qing, P. Chen, and W. Hong, "Substrate integrated waveguide cavity-backed wide slot antenna for 60-GHz bands," *IEEE Trans. Antennas Propag.*, vol. 60, no. 12, pp. 6023–6026, Dec. 2012.
[11] Q. Liao, E. Rajo-Iglesias, and O. Quevedo-Teruel, "*Ka*-band fully metallic TE_{40} slot array antenna with glide-symmetric gap waveguide technology," *IEEE Trans. Antennas Propag.*, vol. 67, no. 10, pp. 6410–6418, Oct. 2019.
[12] N. Bayat-Makou, K. Wu, and A. A. Kishk, "Single-layer substrate-integrated broadside leaky long-slot array antennas with embedded reflectors for 5G systems," *IEEE Trans. Antennas Propag.*, vol. 67, no. 12, pp. 7331–7339, Dec. 2019.
[13] G. P. Le Sage, "3D printed waveguide slot array antennas," *IEEE Access*, vol. 4, pp. 1258–1265, 2016.
[14] A. Gomez-Torrent, M. Garcia-Vigueras, L. Le Coq, A. Mahmoud, M. Ettorre, R. Sauleau, and J. Oberhammer, "A low-profile and high-gain frequency beam steering subterahertz antenna enabled by silicon micromachining," *IEEE Trans. Antennas Propag.*, vol. 68, no. 2, pp. 672–682, Feb. 2020.
[15] J. F. Xu, Z. N. Chen, X. M. Qing, and W. Hong, "Bandwidth enhancement for a 60 GHz substrate integrated waveguide fed cavity array antenna on LTCC," *IEEE Trans. Antennas Progag.*, vol. 59, no. 3, pp. 826–832, Mar. 2011.
[16] Y. Miura, J. Hirokawa, M. Ando, Y. Shibuya, and G. Yoshida, "Double-layer full-corporate-feed hollow-waveguide slot array antenna in the 60-GHz band," *IEEE Trans. Antennas Propag.*, vol. 59, no. 8, pp. 2844–2851, Aug. 2011.
[17] T. Tomura, J. Hirokawa, T. Hirano, and M. Ando, "A wideband 16×16-element corporate-feed hollow-waveguide slot array antenna in the 60-GHz band," *IEICE Trans. Commun.*, vol. E97.B, no. 4, pp. 798–806, 2014.
[18] Z. Shi-Gang, H. Guan-Long, P. Zhao-Hang, and L.-J. Ying, "A wideband full-corporate-feed waveguide slot planar array," *IEEE Trans. Antennas Propag.*, vol. 64, no. 5, pp. 1974–1978, May 2016.
[19] P. Liu, J. Liu, W. Hu, and X. Chen, "Hollow waveguide 32×32-slot array antenna covering 71–86 GHz band by the technology of a polyetherimide fabrication," *IEEE Antennas Wireless Propag. Lett.*, vol. 17, no. 9, pp. 1635–1638, Sep. 2018.
[20] D. Warmowska, K. A. Abdalmalak, L. E. G. Munoz, and Z. Raida, "High-gain, circularly-polarized THz antenna with proper modeling of structures with thin metallic walls," *IEEE Access*, vol. 8, pp. 125223–125233, 2020.
[21] S. A. Razavi, P. S. Kildal, L. Xiang, E. A. Alos, and H. Chen, "2×2-slot element for 60-GHz planar array antenna realized on two doubled-sided PCBs using SIW cavity and EBG-type soft surface fed by microstrip-ridge gap waveguide," *IEEE Trans. Antennas Propag.*, vol. 62, no. 9, pp. 4564–4573, Sep. 2014.
[22] J. Wu, Y. J. Cheng, and Y. Fan, "60-GHz substrate integrated waveguide fed cavity-backed aperture-coupled microstrip patch antenna arrays," *IEEE Trans. Antennas Propag.*, vol. 63, no. 3, pp. 1075–1085, Mar. 2015.
[23] K. Fan, Z. Hao, Q. Yuan, G. Q. Luo, and W. Hong, "A wideband high-gain planar integrated antenna array for E-band backhaul applications," *IEEE Trans. Antennas Propag.*, vol. 68, no. 3, pp. 2138–2147, Mar. 2020.
[24] D.-F. Guan, C. Ding, Z.-P. Qian, Y.-S. Zhang, W.-Q. Cao, and E. Dutkiewicz, "An SIW-based large-scale corporate-feed array antenna," *IEEE Trans. Antennas Propag.*, vol. 63, no. 7, pp. 2969–2976, Jul. 2015.
[25] Y. Cai, Y. Zhang, C. Ding, and Z. Qian, "A wideband multilayer substrate integrated waveguide cavity-backed slot antenna array," *IEEE Trans. Antenna Propag.*, vol. 65, no. 7, pp. 3465–3473, Jul. 2017.
[26] B. Cao, H. Wang, and Y. Huang, "W-band high-gain TE_{220}-mode slot antenna array with gap waveguide feeding network," *IEEE IEEE Antennas Wireless Propag. Lett.*, vol. 15, pp. 988–991, 2016.
[27] D. Zarifi, A. Farahbakhsh, A. U. Zaman, and P. S. Kildal, "Design and fabrication of a high-gain 60-GHz corrugated slot antenna array with ridge gap waveguide distribution layer," *IEEE Trans. Antennas Propag.*, vol. 64, no. 7, pp. 2905–2913, Jul. 2016.
[28] A. Farahbakhsh, D. Zarifi, and A. U. Zaman, "60-GHz groove gap waveguide based wideband H-plane power dividers and transitions: For use in high-gain slot array antenna," *IEEE Trans. Microw. Theory Techn.*, vol. 65, no. 11, pp. 4111–4121, Nov. 2017.
[29] A. Farahbakhsh, D. Zarifi, and A. U. Zaman, "A mmWave wideband slot array antenna based on ridge gap waveguide with 30% bandwidth," *IEEE Trans. Antennas Propag.*, vol. 66, no. 2, pp. 1008–1013, Feb. 2018.
[30] M. Akbari, A. Farahbakhsh, and A.-R. Sebak, "Ridge gap waveguide multilevel sequential feeding network for high-gain circularly polarized array antenna," *IEEE Trans. Antennas Propag.*, vol. 67, no. 1, pp. 251–259, Jan. 2019.
[31] X. Lu, H. Zhang, S. Gu, H. Liu, X. Wang, and W. Lu, "A dual-polarized cross-slot antenna array on a parallel-plate waveguide with compact structure and high efficiency," *IEEE Antennas Wireless Propag. Lett.*, vol. 17, pp. 8–11, 2018.
[32] H. Irie and J. Hirokawa, "Perpendicular-corporate feed in three-layered parallel-plate radiating-slot array," *IEEE Trans. Antennas Propag.*, vol. 65, no. 11, pp. 5829–5836, Nov. 2017.
[33] H. Irie, T. Tomura, and J. Hirokawa, "Perpendicular-corporate feed in a four-layer circularly-polarized parallel-plate slot array," *IEICE Trans. Commun.*, vol. E102.B, no. 1, pp. 137–146, Jan. 2019.
[34] S. Yun, D. Y. Kim, and S. Nam, "Bandwidth and efficiency enhancement of cavity-backed slot antenna using a substrate removal," *IEEE Antennas Wireless Propag. Lett.*, vol. 11, pp. 1458–1461, 2012.
[35] S. Yun, D. Y. Kim, and S. Nam, "Bandwidth enhancement of cavity-backed slot antenna using a via-hole above the slot," *IEEE Antennas Wireless Propag. Lett.*, vol. 11, pp. 1092–1095, 2012.
[36] S. Ji, T. Tomura, and J. Hirokawa, "Fast analysis and bandwidth enhancement of the radiating subarray by method of moments for a parallel-plate slot array antenna with perpendicular-corporate feed," *IEEE Trans. Antennas Propag.*, early access, Oct. 15, 2021, doi: 10.1109/TAP.2021.3119059.
[37] S. Ji, T. Tomura, and J. Hirokawa, "Efficient optimization for bandwidth of the element of a multilayer parallel-plate slot array," in *Proc. Int. Symp. Antennas Propag.*, Jan. 2021, pp. 2–4.
[38] D. R. Jackson, C. Caloz, and T. Itoh, "Leaky-wave antennas," *Proc. IEEE*, vol. 100, no. 7, pp. 2194–2206, Jul. 2012.
[39] G. Lovat, P. Burghignoli, and D. R. Jackson, "Fundamental properties and optimization of broadside radiation from uniform leaky-wave antennas," *IEEE Trans. Antennas Propag.*, vol. 54, no. 5, pp. 1442–1452, May 2006.
[40] N. Marcuvitz, "Inductive posts," in *Waveguide Handbook*, vol. 21. Maricourt, France: Peter Pregrinunus, 1986, ch. 5, pp. 280–286.
[41] X. Xu, M. Zhang, J. Hirokawa, and M. Ando, "E-band plate-laminated waveguide filters and their integration into a corporate-feed slot array antenna with diffusion bonding technology," *IEEE Trans. Microw. Theory Techn.*, vol. 64, no. 11, pp. 3592–3603, Nov. 2016.

SHUANG JI was born in Jiangsu, China, in 1993. She received the B.S. degree in information countermeasure technology and the M.S. degree in electronic and communication engineering from the Nanjing University of Science and Technology, Nanjing, China, in 2015 and 2018, respectively. She is currently pursuing the Ph.D. degree in electrical and electronic engineering with the Tokyo Institute of Technology, Tokyo, Japan.

Her current research interests include electromagnetic analysis and planar waveguide slot array antennas.

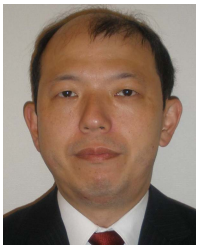

JIRO HIROKAWA (Fellow, IEEE) was born in Tokyo, Japan, in 1965. He received the B.S., M.S., and D.E. degrees in electrical and electronic engineering from the Tokyo Institute of Technology (Tokyo Tech), Tokyo, Japan, in 1988, 1990, and 1994, respectively.

He was a Research Associate and an Associate Professor with Tokyo Tech, from 1990 to 1996 and, from 1996 to 2015, respectively, where he is currently a Professor. He was a Postdoctoral Fellow with the Antenna Group, Chalmers University of Technology, Gothenburg, Sweden, from 1994 to 1995. He has authored or coauthored more than 200 peer-reviewed journal articles and more than 600 international conference presentations. His current research interests include analyses, designs, fabrication techniques of slotted waveguide array antennas, millimeter-wave, terahertz antennas, and beam-switching circuits.

Dr. Hirokawa is a fellow of IEICE. He received the IEEE AP-S Tokyo Chapter Young Engineer Award, in 1991, the Young Engineer Award from IEICE, in 1996, the Tokyo Tech Award for Challenging Research, in 2003, the Young Scientists' Prize from the Ministry of Education, Cultures, Sports, Science and Technology in Japan, in 2005, the Best Paper Award, in 2007, the Best Letter Award from IEICE Communications Society, in 2009, and the IEICE Best Paper Award, in 2016 and 2018. He was the Chair of the Technical Program Committee for ISAP 2016 and the Chair of IEICE Technical Committee on Antennas and Propagation, from 2017 to 2019. He served as an Associate Editor for *IEICE Transactions on Communications*, from 1999 to 2003 and, from 2004 to 2007. He also served as an Associate Editor, from 2013 to 2016, and has been serving as a Track Editor for IEEE TRANSACTIONS ON ANTENNAS AND PROPAGATION, since 2016.

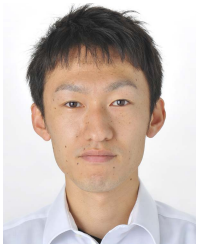

TAKASHI TOMURA (Member, IEEE) received the B.S., M.S., and D.E. degrees in electrical and electronic engineering from the Tokyo Institute of Technology, Tokyo, Japan, in 2008, 2011, and 2014, respectively. He was a Research Fellow with the Japan Society for the Promotion of Science (JSPS), in 2013. From 2014 to 2017, he has worked with Mitsubishi Electric Corporation, Tokyo, where he was engaged in research and development of aperture antennas for satellite communications and radar systems. From 2017 to 2019, he was a Specially Appointed Assistant Professor with the Tokyo Institute of Technology, where he is currently an Assistant Professor. His research interests include electromagnetic analysis, aperture antennas, and planar waveguide slot array antennas.

He is a member of the IEICE. He received the Best Student Award from Ericsson Japan, in 2012, the IEEE AP-S Tokyo Chapter Young Engineer Award, in 2015, and the Young Researcher Award from IEICE Technical Committee on Antennas and Propagation, in 2018.